Journal of Power Sources 195 (2010) 2118–2124

Contents lists available at ScienceDirect

Journal of Power Sources

journal homepage: www.elsevier.com/locate/jpowsour

Mesoporous activated carbon fiber as electrode material for high-performance electrochemical double layer capacitors with ionic liquid electrolyte

Bin Xu[a,b,*], Feng Wu[b], Renjie Chen[b], Gaoping Cao[a], Shi Chen[b], Yusheng Yang[a]

[a] Research Institute of Chemical Defense, Beijing 100083, China
[b] School of Chemical Engineering & Environment, Beijing Institute of Technology, Beijing 100081, China

ARTICLE INFO

Article history:
Received 30 June 2009
Received in revised form 30 August 2009
Accepted 30 September 2009
Available online 14 October 2009

Keywords:
Electrochemical double layer capacitor
Activated carbon fiber
Mesopore
Ionic liquid
Capacitance

ABSTRACT

Activated carbon fibers (ACFs) with super high surface area and well-developed small mesopores have been prepared by pyrolyzing polyacrylonitrile fibers and NaOH activation. Their capacitive performances at room and elevated temperatures are evaluated in electrochemical double layer capacitors (EDLCs) using ionic liquid (IL) electrolyte composed of lithium bis(trifluoromethane sulfone)imide ($LiN(SO_2CF_3)_2$) and 2-oxazolidinone ($C_3H_5NO_2$). The surface area of the ACF is as high as 3291 $m^2\,g^{-1}$. The pore volume of the carbon reaches 2.162 $cm^3\,g^{-1}$, of which 66.7% is the contribution of the small mesopores of 2–5 nm. The unique microstructures enable the ACFs to have good compatibility with the IL electrolyte. The specific capacitance reaches 187 $F\,g^{-1}$ at room temperature with good cycling and self-discharge performances. As the temperature increases to 60 °C, the capacitance increases to 196 $F\,g^{-1}$, and the rate capability is dramatically improved. Therefore, the ACF can be a promising electrode material for high-performance EDLCs.

1. Introduction

Electrochemical double layer capacitors (EDLCs) have attracted considerable attention as a novel energy-storage device with high power density and long cycling durability. EDLCs are now widely used in memory back-up systems, uninterruptable power sources, portable electronics, *etc.*, and will find large-scale applications in hybrid electric vehicles (HEVs) by coupling with fuel cells or secondary batteries to deliver high power for vehicle acceleration and to store the energy converted from braking [1,2]. Nowadays research is mainly focused on improving the energy density and temperature limit of the EDLCs [3–5].

Activated carbons are often used as electrode materials in EDLCs because they can be prepared with large specific surface areas and are commercially available and cheap [6–10]. Theoretically, the higher is the specific surface area of the carbon, the stronger will be its ability to accumulate charges. However, specific capacitance does not necessarily increase proportionally to the surface area of the porous carbon. The size of the pores is another critical factor strongly affecting the capacitance of the carbon. The carbon becomes hardly accessible if its pores are smaller than the solvated ions [11]. Therefore, a good match between the pore size in the carbon material and the dimension of the ionic species is important for achieving high specific capacitance [12,13]. In addition, it has been confirmed that size of the mesopores and their interconnectivity of the carbon strongly influence the dynamic properties of the EDLCs [14–17]. Therefore, it is important to design carbon materials with pores large enough for the electrolyte to access freely but, in the meantime, small enough to ensure a large surface area [18]. Carbon materials with small mesopore (2–5 nm in size, larger than the size of two solvated ions) are believed to be superior in constructing EDLCs with high energy density and high power density [3].

Increase of the operation voltage of a capacitor leads to a significant enhancement of energy and power densities. Replacing the aqueous electrolyte with organic ones is an easy way to increase the operation voltage of the capacitor. Actually the cutting-edge supercapacitors on the market are using non-aqueous electrolytes. A drawback of these aprotic electrolytes is that the organic solvents cannot meet the requirements of environmental compatibility and safety due to vapor generation, flammability and explosion, especially for application in HEV. Ionic liquid (IL) is expected to be an alternative to the traditional non-aqueous electrolyte due to its wide electrochemical window and high safety at high temperatures.

EDLCs with IL electrolyte can work at higher voltages and have higher safety and better capacity retention at high temperatures than those using non-aqueous electrolytes [19–22]. We previously reported that ILs composed of lithium bis(trifluoromethane sulfonyl) imide ($LiN(SO_2CF_3)_2$, LiTFSI) and 2-oxazolidinone ($C_3H_5NO_2$, OZO) could be easily prepared and showed high thermal stability, high electrochemical stability and excellent electrochemical performances as electrolyte for EDLCs [23]. However, the capacitance

* Corresponding author. Fax: +86 10 68451429.
E-mail addresses: xubinn@sohu.com, xubin@bit.edu.cn (B. Xu).

0378-7753/$ – see front matter © 2009 Elsevier B.V. All rights reserved.
doi:10.1016/j.jpowsour.2009.09.077

of the activated carbon with a surface area of 1200 $m^2 g^{-1}$ in that IL was only 33 $F g^{-1}$. This is attributed to the dominant micropores in the carbon where the IL ions cannot access. Therefore, carbon materials with suitable pore distribution are required to match the IL electrolyte in order to optimize the performance of the EDLCs.

Chemical activation with alkali hydroxide (KOH or NaOH) is an effective method to prepare activated carbons with very high surface area and microporous structures [24–26]. Although the pore size can be controlled to some extent by optimizing the precursors and the activation conditions, the micropores are dominant in the carbons. In this paper, polyacrylonitrile (PAN) fibers were pyrolyzed and then activated with NaOH. By controlling the content of NaOH impregnated in the carbonized fiber, small-mesopore dominated (2–5 nm) activated carbon fibers (ACFs) with super high surface area were prepared. This paper is to characterize the microstructures of the activated carbon and evaluate their electrochemical performances at various temperatures and current densities in EDLCs with IL electrolyte.

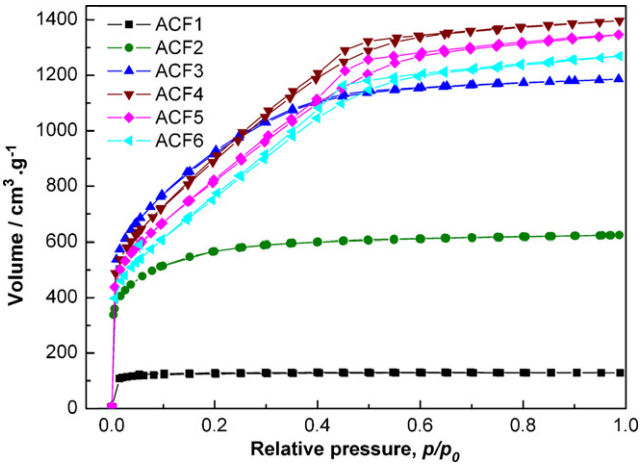

Fig. 1. N_2 (77K) adsorption/desorption isotherms of the ACF samples.

2. Experimental

2.1. Preparation and characterization of ACFs

Commercial PAN fiber was used as the starting material. After pre-oxidized at 240 °C in air for 4 h, the fiber was heated up to 600 °C at a rate of 10 °C min^{-1} in a tubular furnace in N_2 (99.999%) and kept there for 1 h. Then the carbonized fiber (CF) was soaked in concentrated NaOH solution under vacuum for several hours. The weight ratio of NaOH to the CF (*R* value) varied between 1 and 6. After dried at 150 °C for 5 h, the fiber in NaOH was activated at 600 °C for 1 h in a tubular furnace under N_2 (99.999%) atmosphere. The activated material was washed with 0.5 mol L^{-1} HCl and distilled water in sequence to remove the residual NaOH completely. After dried at 120 °C for 12 h, the final ACFs were obtained. The ACF samples prepared at a weight ratio of NaOH/CF = *R* is denoted as ACF*R*.

The specific surface area and pore structure of the ACF were determined with the nitrogen adsorption/desorption isotherms at 77 K (Quantachrome NOVA 1200). All the samples were degassed at 300 °C for 8 h prior to the adsorption experiments. The specific surface area was calculated by the conventional Brunauer–Emmett–Teller (BET) method. The total pore volume was estimated by the amount of adsorbed N_2 at a relative pressure of 0.99. The distribution of the pore size of the samples was calculated by the density functional theory (DFT) method.

2.2. Ionic liquid electrolyte

The IL composed of LiTFSI and OZO at a molar ratio of 1:4.5 was used as the electrolyte. The details for the synthesis of the IL electrolyte have been described in our previous paper [23]. The properties of the IL electrolyte are listed in Table 1.

2.3. Evaluation of capacitive performance

Electrodes were prepared by pressing the mixture of 87 wt% ACF, 10 wt% acetylene black and 3 wt% PTFE binder into pellets (11 mm in diameter), followed by drying under vacuum at 120 °C for 12 h. A button-type capacitor was assembled with two carbon electrodes separated by polypropylene membrane using the IL as the electrolyte in an Ar-filled glovebox (MBraun LabMaster 130).

The electrochemical performance of the test capacitors was evaluated by cyclic voltammetry (CV) on a Solatron 1280B electrochemical workstation and galvanostatic charge/discharge between 0 and 2 V on an Arbin cell tester (CT2001A).

3. Results and discussion

3.1. Preparation and microstructure of ACF

The physical and electrochemical properties of the ACF are dependent on the *R* value. ACFs with different pore structures were prepared by varying the *R* value between 1 and 6.

Fig. 1 shows the N_2 adsorption/desoption isotherms of the ACFs at 77 K. The shape of the isotherms varies remarkably with the *R* value. The isotherms of ACF1 and ACF2 are both type I according to the IUPAC classification. The knee of the isotherms appears at very low relative pressure ($p/p_0 < 0.05$) and the plateau is fairly flat, characteristic of their microporous features. Different from ACF1 and ACF2, the isotherms of ACF3 have a glacis knee and the slope of the plateau increases due to multi-layer adsorption, suggesting the coexistence of larger micropores and mesopores in the material. When *R* increases to 4 and over, the adsorption volume of the carbons proportionally increases with the relative pressure until $p/p_0 \approx 0.5$. The widely opened knees and the slight hysteresis loops at the relative pressure of 0.3–0.6 indicate the presence of a considerable amount of small mesopores in these samples.

The pore features of the ACF as a function of *R* value are shown in Fig. 2. It is seen that the BET surface area of the ACF increases from 498 $m^2 g^{-1}$ at *R* = 1 to 3291 $m^2 g^{-1}$ at *R* = 4. Then it decreases slightly as *R* further increases. The dependence of the total pore volume on the *R* value is similar to that of the BET surface area. It reaches a maximum of 2.162 $cm^3 g^{-1}$ at *R* = 4, indicating that the porous structure of the material is well developed. However, the dependences of the volume of the micropores and the mesopores on *R* are different. The mesopore volume keeps increasing with increasing *R* values. In contrast, the volume of the micropores turns to decrease after *R* > 3. This means that more micropores expand to mesopores at high

Table 1
Properties of the IL electrolyte composed of LiTFSI and OZO.

Molar ratio of LiTFSI:OZO	Eutectic temperature (°C)	Decom. temperature (°C)	Electrochem. window (V)	Conductivity (mS cm^{-1})				
				0	25	40	60	80
1:4.5	−60.9	232.7	3.0	0.143	0.753	1.61	3.50	6.19

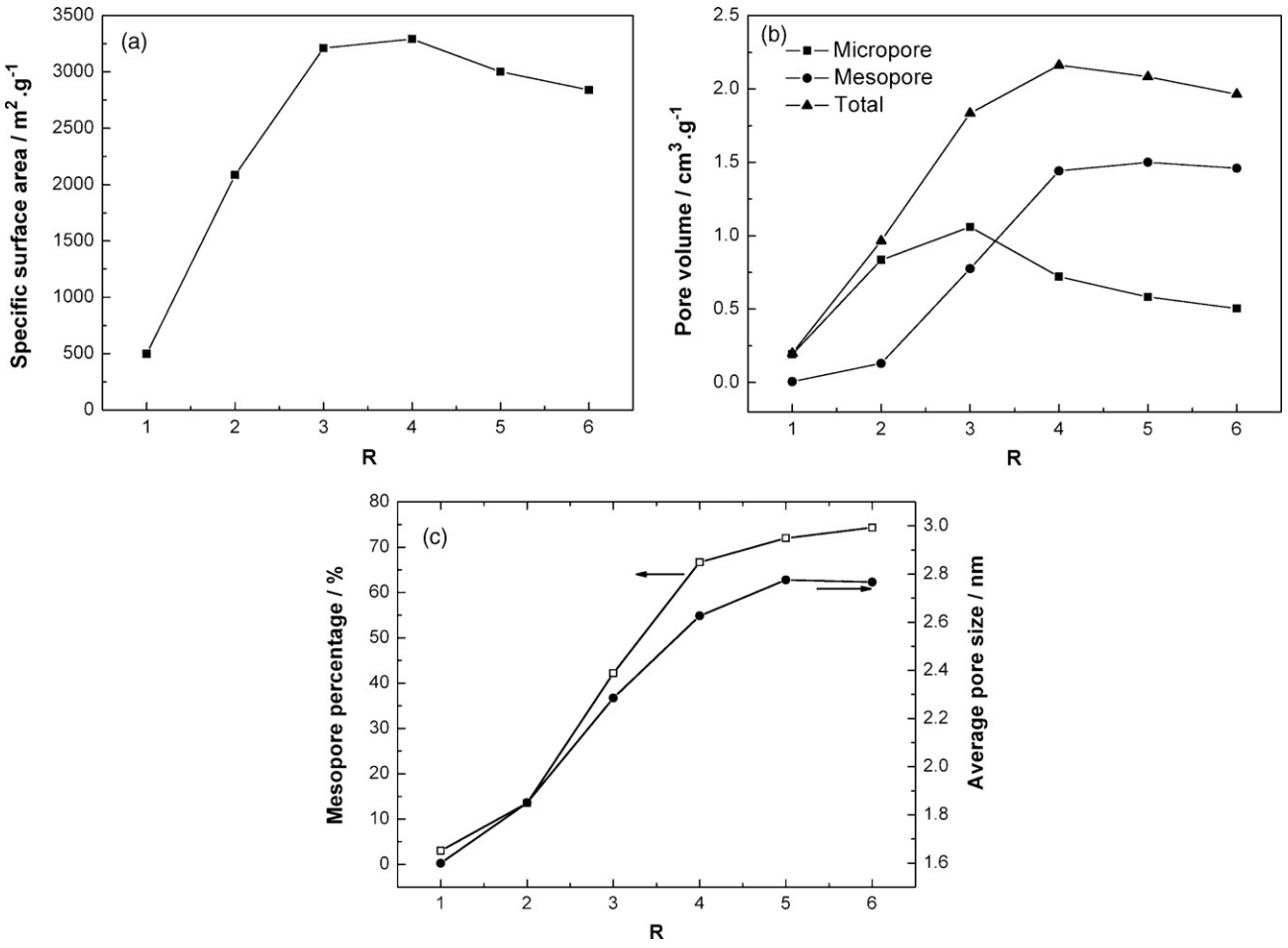

Fig. 2. The pore features of the ACF samples as a function of the *R*.

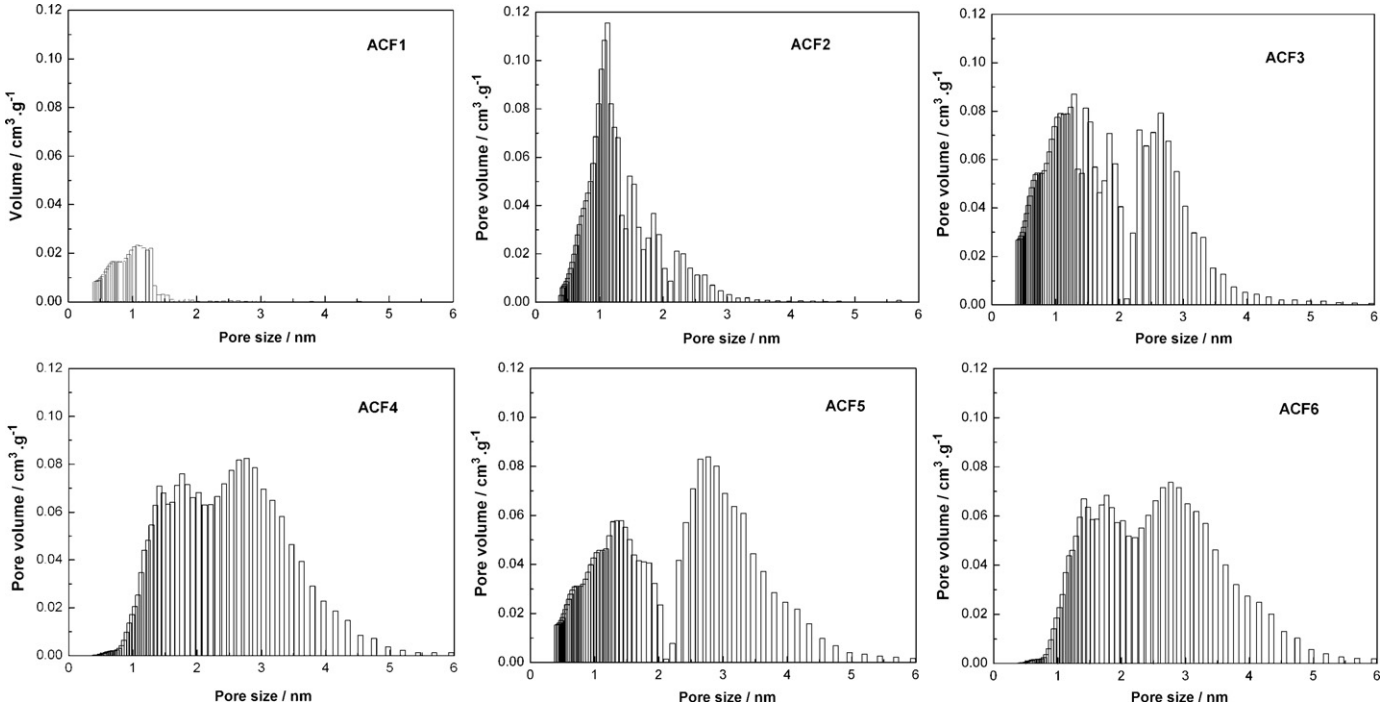

Fig. 3. . Pore size distribution of the ACF samples calculated by DFT method.

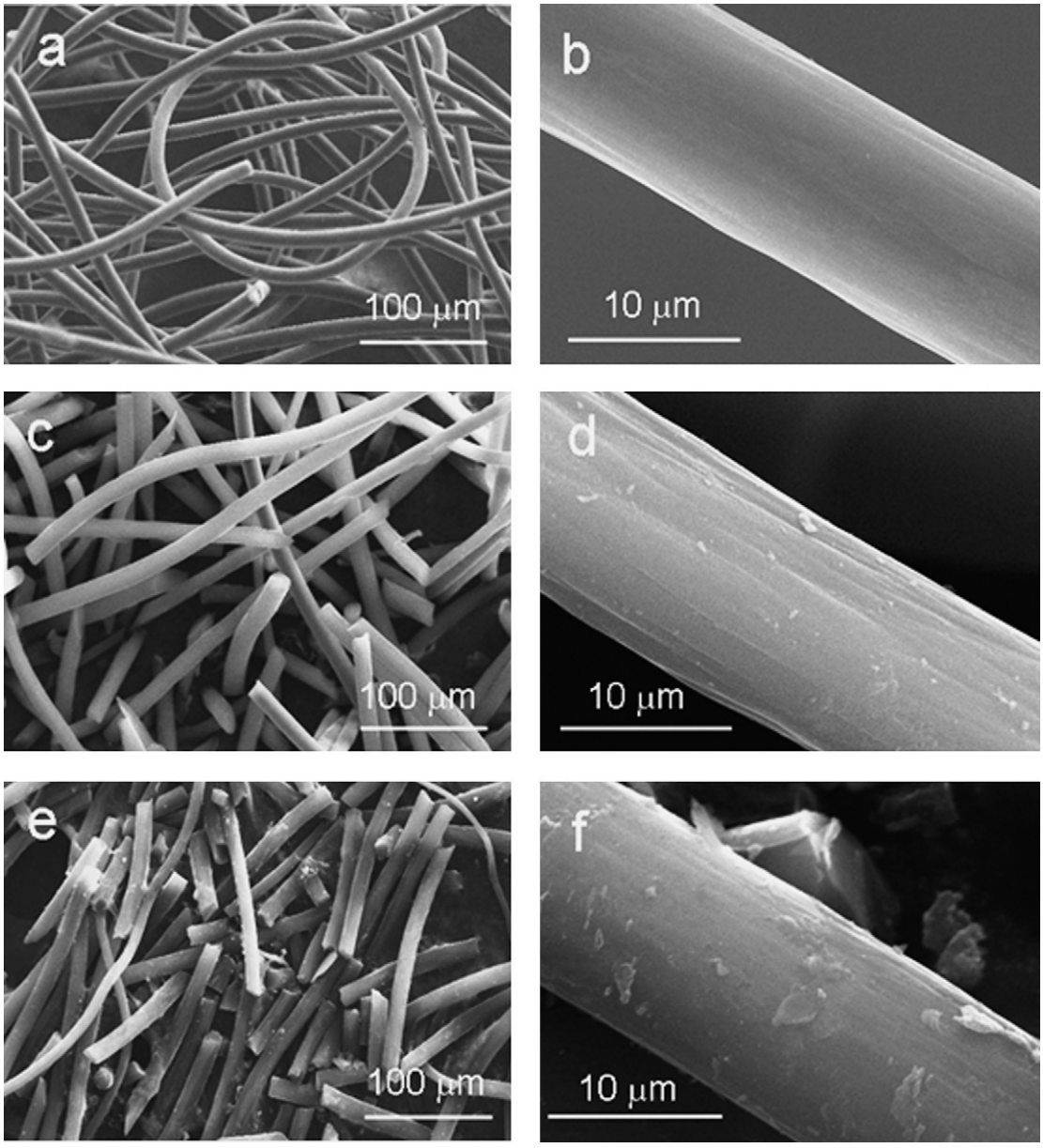

Fig. 4. SEM imagines of ACF1: a and b; ACF3: c and d; ACF5: e and f.

R values. As a result, the content of the mesopores (the ratio of the mesopore volume to the total pore volume) increases with increasing *R*. At $R = 3$, the mesopores contribute almost half of the total pore volume. At $R > 3$, the contribution of the mesopores becomes dominant in the total pore volume. The average pore size also increases with the *R* value. The ACF samples at $R \geq 3$ possess both high specific surface area and well-developed mesoporous structure, indicating that the ACF is an attractive candidate of EDLC electrode material.

Fig. 3 shows the distribution of the pore size in the ACF calculated by the density function theory (DFT) method. As the *R* value increases, the pore size distribution becomes wider. The distributions of the pore sizes of ACF1 and ACF2 are unimodal. The size of most of the pores is *ca.* 1 nm. At $R \geq 3$, the ACF samples have a more dispersed pore size distribution over the wider range from 0.5 to 5 nm with a bimodal feature at ~1.5 and ~3 nm.

Porous carbon fiber was obtained after the char was etched off with NaOH at high temperature. Fig. 4 presents the surface morphology of the ACF. The shape of the PAN fiber is well kept when the *R* value is low (ACF1). With increasing NaOH content for the activation, the damage to the precursor fiber becomes obvious. Although ACF3 roughly reserves a fibrous feature, the fiber become short and their surfaces are rough. As the *R* increases to 5, the fiber is severely damaged and the surface becomes very rough.

Two processes are involved in chemical activation, the pore formation and pore widening [24]. Pore widening usually begins when a number of opened pores are created and the chemical activation agent is abundant inside the pores. In this work, some micropores are expanded to mesopores at $R \geq 3$. Therefore, the mesopore volume increases while the micropore volume decreases. As the *R* value is further increased, the abundant alkali etches off the walls of some pores entirely, resulting in a slight decrease of the specific surface area and the total pore volume. One porous material cannot be characteristic of both high specific surface area and large pore size. In this work, however, ACFs with both high surface area and mesoprous structure were obtained by optimizing the activation

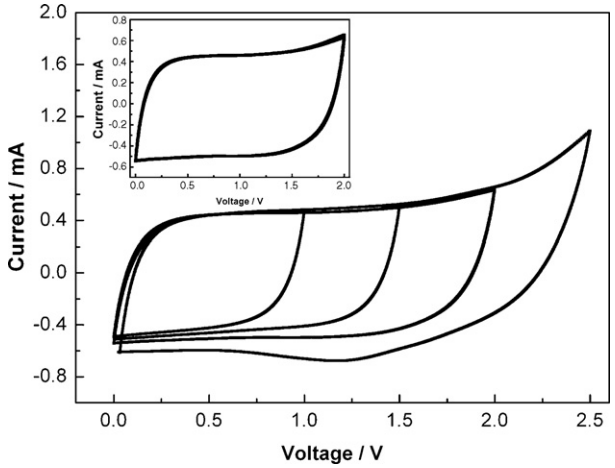

Fig. 5. Typical CV curves of the ACF-based EDLCs (ACF6 is used here) using IL electrolyte in different potential ranges (inset: CV curves in 0–2 V), scan rate: 1 mV s^{-1}.

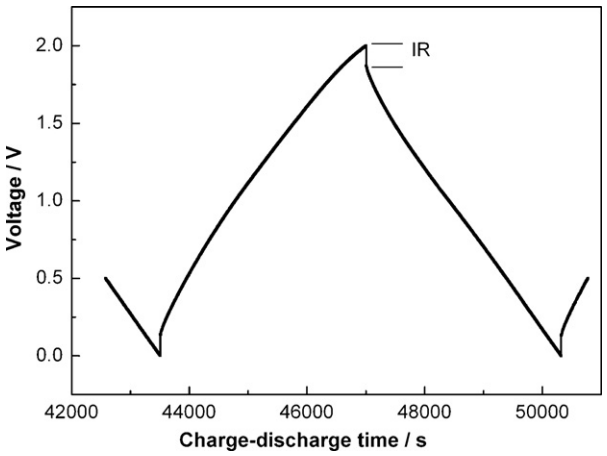

Fig. 6. Charge–discharge curves of an ACF6-based EDLC using IL electrolyte (current density 50 mA g^{-1}).

condition.

3.2. Electrochemical performances of ACF in IL electrolyte

EDLCs were assembled with the ACF as the electrode and the IL as the electrolyte. Fig. 5 shows the typical CV curves of the EDLC in different potential ranges. A weak oxidation peak appears when the cutoff charge voltage increases to 2.5 V. Therefore, the cutoff charge voltage of the EDLC was set to be 2.0 V in the subsequent tests. The well-defined rectangular CV curves in the range of 0–2 V demonstrate the typical capacitive behavior of the ACF electrodes.

Galvanostatic charge–discharge cycling is performed to evaluate the capacitance of the ACFs. Fig. 6 shows the typical charge–discharge profiles of the ACF samples in the IL electrolyte at room temperature. The linear voltage–time dependence demonstrates the typical capacitive behavior of the cell. The sharp voltage change at the beginnings of the charge and discharge processes is related to the equivalent series resistance (ESR) of the capacitor ($\Delta V = IR$). The relative high ESR of the capacitor is attributed to the low ionic conductivity of the IL electrolyte at room temperature.

The dependence of the capacitance of the ACF at 50 mA g^{-1} on the R value is plotted in Fig. 7(a). Sample ACF1 with a surface area of 498 m^2 g^{-1} shows very low capacitance (0.7 F g^{-1}). Even when the surface area increases to 2085 m^2 g^{-1} (ACF2), the capacitance of the material is still low (54 F g^{-1}). Previous studies show that the capacitance of ACF2 electrode is as high as 180 F g^{-1} in a $LiClO_4$/PC electrolyte (PC for propylene carbonate) [10]. Clearly the low capacitance of ACF2 in the IL electrolyte is due to the large ions of the IL electrolyte. Micropores are dominant in ACF1 and ACF2 but are too small for the large IL ions to access.

The capacitance of the ACF in the IL electrolyte increases dramatically when the mesopores become predominant in the carbon of $R \geq 3$. The capacitance of ACF4 is as high as 188 F g^{-1}, close to its capacitance in $LiClO_4$/PC electrolyte. This implies that the pores in ACF4 have been sufficiently expanded for the large ions in the IL to access. The strong dependence of the capacitance on the pore size of the ACF confirms that the matching of the pore size of the carbon electrode with the ion size of the electrolyte is critical for the performance of the EDLCs [13]. The capacitance of the ACF at $R > 3$ is also much higher than that of the carbons (80–120 F g^{-1}) in traditional non-aqueous electrolyte [27]. The extraordinarily high capacitance of the ACF in the IL electrolyte is attributed to the unique microstructures of the ACFs, *i.e.* the highly accessible mesoporous structure and super high surface area.

Fig. 7(b) shows that the capacitance per surface area increases from 0.14 μF cm^{-2} at $R = 1$ to 5.7 μF cm^{-2} at $R = 4$ and finally to 6.5 μF cm^{-2} at $R = 6$. This variation agrees with that of the average pore size of the carbon (Fig. 2c). As the R value increases, the pore widening process becomes dominant, resulting in the increase of the average pore size. As more pores become sufficiently large for

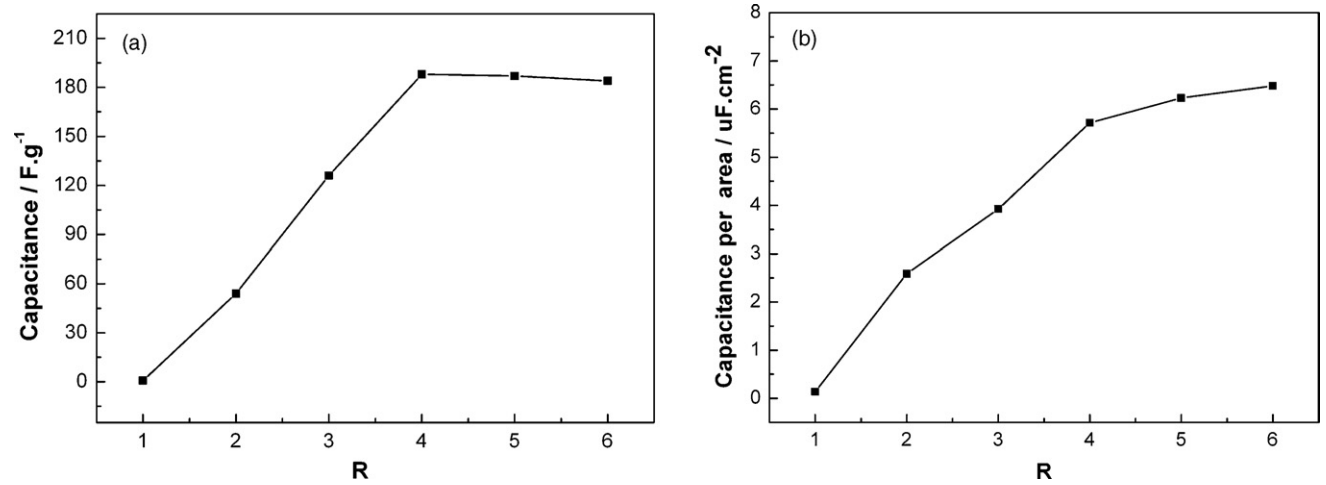

Fig. 7. Specific capacitance (a) and capacitance per area (b) of the ACF in IL electrolyte as a function of R value.

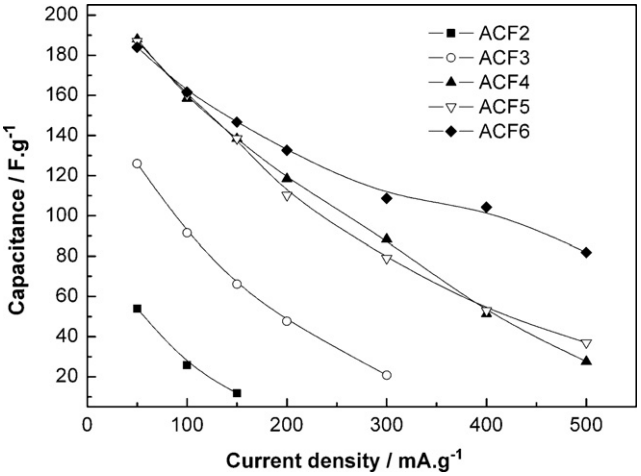

Fig. 8. Rate performance of the ACF in IL electrolyte.

the IL electrolyte to access, the capacitance per area increases. This confirms that the mesopores are more efficient than the micropores in contributing to the electric double layer capacitance, especially when electrolyte with large ions is applied.

Fig. 8 presents the rate performance of the ACFs. The specific capacitance of all the ACFs decreases with increasing current density. The larger is the pore, the easier will it be for the ions to get in and out of the pores. Hence the carbon prepared at larger *R* value exhibits better rate performance. The sample ACF6 shows the best rate performance because of its highly mesoporous structure (Fig. 3). At a current density of 500 mA g^{-1}, the specific capacitance of ACF6 is still as high as 82 F g^{-1}.

Fig. 9 shows the typical cycling performance of an EDLC with ACF electrodes at room temperature (current density 350 mA g^{-1}). Excellent capacitance retention is obtained over prolonged cycling test. The capacity decay is only 10% in 500 cycles. Fig. 10 shows the typical self-discharge performance of the capacitor at room temperature. The voltage of the capacitor drops from 2.0 V to *ca.* 1.6 V in 24 h, while the voltage of the EDLCs with IL electrolyte LiTFSI-acetamide at a molar ratio of 1:6 drops from 2.0 V to 1.4 V during 3.3 h [22].

The low volatility and high thermal stability of the IL electrolyte permit it to work at high temperatures. Meanwhile, the resistance of the electrolyte, sensitive to temperature, strongly affects the rate performance of the capacitor. Therefore, EDLCs using IL electrolyte are expected to have improved rate performance and higher capacitance at high temperatures. Fig. 11 indicates that the sharp voltage drop at the beginning of discharge decreases remarkably, from 0.255 V at 25 °C to 0.161 V at 40 °C and 0.084 V at 60 °C. The

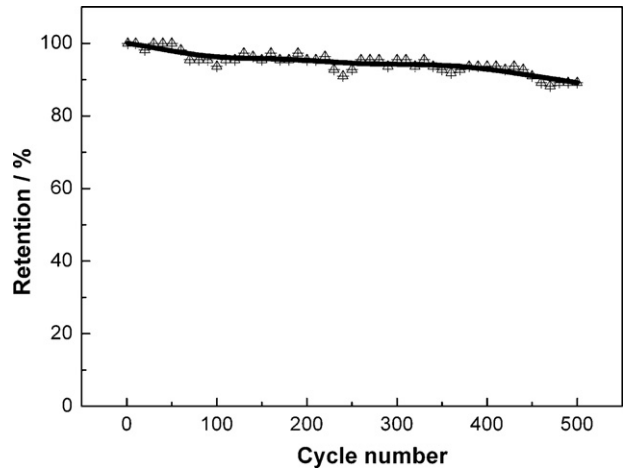

Fig. 9. Cycle performance of an ACF-based EDLC using IL electrolyte at 350 mA g^{-1} rate.

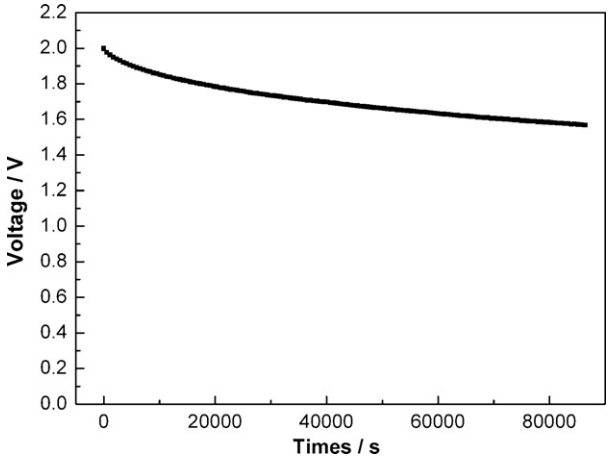

Fig. 10. Self-discharge performance of an ACF-based EDLC using IL electrolyte.

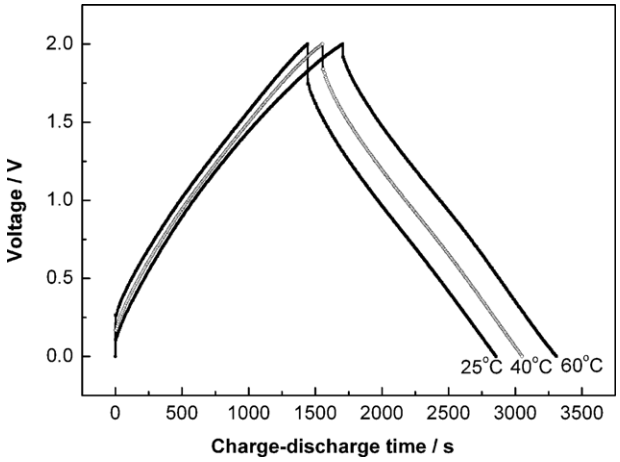

Fig. 11. Charge–discharge curves of ACF5-based EDLC using IL electrolyte at different temperatures at a current density of 100 mA g^{-1}.

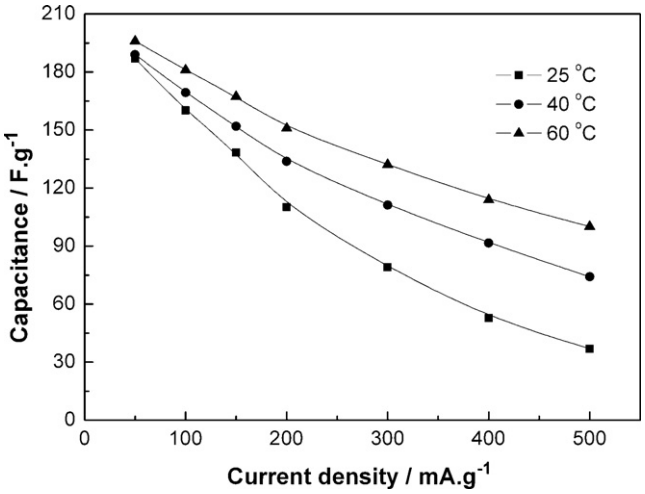

Fig. 12. Comparison of the rate performance of ACF5 in IL electrolyte at various temperatures.

decrease of the sharp drop is attributed to the increased conductivity of the IL electrolyte at elevated temperature (Table 1). As a result, the specific capacitance of ACF5 increases from 160 F g^{-1} at 25 °C to 169 F g^{-1} at 40 °C and 181 F g^{-1} at 60 °C.

Fig. 12 shows the rate performances of the ACF5-based capacitors at different temperatures. As the temperature increases from 25 to 60 °C, the rate capability is dramatically improved. The capacitance of ACF5 increases from 39 F g^{-1} at 25 °C to 100 F g^{-1} at 60 °C at a current density of 500 mA g^{-1}. The enhanced rate performance at elevated temperatures is mainly attributed to the increasing mobility of the ions in the IL electrolyte. In contrast, the performances of EDLCs with conventional organic electrolyte cannot work at such high temperatures due to the volatility and flammability of the organic solvent.

4. Conclusions

ACFs with super high surface area and highly mesoporous structure have been prepared and evaluated as electrode materials for EDLCs using LiTFSI-OZO ionic liquid electrolyte. The BET surface area of the ACF is as high as 3291 m^2 g^{-1}. The pore volume of the carbon reaches 2.162 cm^3 g^{-1}, of which 66.7% is the contribution of the small mesopores of 2–5 nm. The unique microstructures enable the ACFs to have good compatibility with the IL electrolyte. The specific capacitance reaches 187 F g^{-1} at room temperature. The EDLC also shows good cycling and self-discharge performances. As the temperature increases to 60 °C, the capacitance increases to 196 F g^{-1}, and the rate capability is dramatically improved. Therefore, the ACF can be a promising electrode material for high-performance EDLCs.

Acknowledgements

This work was financially supported by the National Science Foundation of China (NSFC, 20633040 and 50802112), the National 863 Program (2006AA11A165) and the National Key Basic Research and Development Program (2009CB220100).

References

[1] R. Kötz, M. Carlen, Electrochim. Acta 45 (2000) 2483–2498.
[2] M. Mastragostino, F. Soavi, J. Power Sources 174 (2007) 89–93.
[3] P. Simon, Y. Gogotsi, Nat. Mater. 7 (2008) 845–854.
[4] B. Xu, F. Wu, S. Chen, Z. Zhou, G. Cao, Y. Yang, Electrochim. Acta 54 (2009) 2185–2189.
[5] A. Balducci, R. Dugas, P.L. Taberna, P. Simon, D. Plée, M. Mastragostino, S. Passerini, J. Power Sources 165 (2007) 922–927.
[6] E. Frackowiak, Phys. Chem. Chem. Phys. 9 (2007) 1774–1785.
[7] K.P. Wang, H. Teng, Carbon 44 (2006) 3218–3225.
[8] G. Lota, T.A. Centeno, E. Frackowiak, F. Stoeckli, Electrochim. Acta 53 (2008) 2210–2216.
[9] M.J. Bleda-Martínez, D. Lozano-Castelló, E. Morallón, D. Cazorla-Amorós, A. Linares-Solano, Carbon 44 (2006) 2642–2651.
[10] B. Xu, F. Wu, R. Chen, G. Cao, S. Chen, Z. Zhou, Y. Yang, Electrochem. Commun. 10 (2008) 795–797.
[11] H. Yamada, H. Nakamura, F. Nakahara, I. Moriguchi, T. Kudo, J. Phys. Chem. C 111 (2007) 227–233.
[12] C.O. Ania, J. Pernak, F. Stefaniak, E. Raymundo-Pinéro, F. Béguin, Carbon 44 (2006) 3113–3148.
[13] H. Liu, G. Zhu, J. Power Sources 171 (2007) 1054–1061.
[14] H.Q. Li, R.L. Liu, D.Y. Zhao, Y.Y. Xia, Carbon 45 (2007) 2628–2635.
[15] A.B. Fuertes, G. Lota, T.A. Centeno, E. Frackowiak, Electrochim. Acta 50 (2005) 2799–2805.
[16] K. Xia, Q. Gao, J. Jiang, J. Hu, Carbon 46 (2008) 1718–1726.
[17] D.W. Wang, F. Li, M. Liu, G.Q. Lu, H.M. Cheng, Angew Chem. Int. Ed. 47 (2008) 373–376.
[18] J. Chmola, G. Yushin, R.K. Dash, E.N. Hoffman, J.E. Fischer, M.W. Barsoum, Y. Gogotsi, Electrochem. Solid-State Lett. 8 (2005) A357–A360.
[19] T. Sato, G. Masuda, K. Takagi, Electrochim. Acta 49 (2004) 3603–3611.
[20] B. Xu, F. Wu, R. Chen, G. Cao, S. Chen, G. Wang, Y. Yang, J. Power Sources 158 (2006) 773–778.
[21] E. Frackowiak, G. Lota, J. Pernak, Apll. Phys. Lett. 86 (2005), 164104-1-3.
[22] R. Chen, F. Wu, B. Xu, L. Li, X. Qiu, S. Chen, J. Electrochem. Soc. 154 (2007) A703–A708.
[23] R. Chen, F. Wu, B. Xu, L. Li, X. Qiu, S. Chen, J. Phys. Chem. C 111 (2007) 5184–5194.
[24] M. Wu, Q. Zha, J. Qiu, Y. Guo, H. Shang, A. Yuan, Carbon 42 (2004) 205–210.
[25] R.L. Tseng, S.K. Tseng, J. Colloid Interface Sci. 287 (2005) 428–437.
[26] M.A. Lillo-Ródenas, D. Lozano-Castelló, D. Cazorla-Amorós, A. Linares-Solano, Carbon 39 (2001) 751–759.
[27] A. Burke, Electrochim. Acta 53 (2007) 1083–1091.